Aerosol and Air Quality Research, 15: 1613–1626, 2015

ISSN: 1680-8584 print / 2071-1409 online
doi: 10.4209/aaqr.2014.12.0310

Fugitive Particulate Matter Emissions to the Atmosphere from Tracked and Wheeled Vehicles in a Desert Region by Hybrid-Optical Remote Sensing

Wangki Yuen[1], Ke Du[2], Sotiria Koloutsou-Vakakis[1], Mark J. Rood[1*], Byung J. Kim[1,3], Michael R. Kemme[3], Ram A. Hashmonay[4], Chad Meister[5]

[1] *University of Illinois, 205 N. Mathews Ave., Urbana, IL 61801, USA*
[2] *University of Calgary, 2500 University Dr. NW, Calgary, AB T2N 1N4, Canada*
[3] *ERDC-CERL, 2902 Newmark Dr., Champaign, IL 61826, USA*
[4] *Atmosfir Optics Ltd., 8801 Fast Park Dr., Suite 301, Raleigh, NC 27617, USA*
[5] *Fort Carson, 7335 Womack St., Fort Carson, CO 80913, USA*

ABSTRACT

A hybrid-optical remote sensing (hybrid-ORS) method was developed to quantify mass emission factors (EFs) for fugitive particulate matter with aerodynamic diameters ≤ 10 µm (PM_{10}) and ≤ 2.5 µm ($PM_{2.5}$). In-situ range-resolved extinction coefficient and concurrent point measurements of PM_{10} and $PM_{2.5}$ mass concentrations are used to quantify two-dimensional (2-D) PM_{10} and $PM_{2.5}$ mass concentration profiles. Integration of each 2-D mass concentration profile with wind data, event duration, and source type provides the corresponding fugitive PM_{10} and $PM_{2.5}$ EFs. This method was used to quantify EFs for fugitive PM_{10} and $PM_{2.5}$ emitted from tracked and wheeled vehicles travelling on unpaved roads in a desert region. The EFs for tracked vehicles ranged from 206 g/km to 1,738 g/km for PM_{10} and from 78 g/km to 684 g/km for $PM_{2.5}$, depending on vehicle speed and vehicle type. The EFs for the wheeled vehicle ranged from 223 g/km to 4,339 g/km for PM_{10} and from 44 g/km to 1,627 g/km for $PM_{2.5}$. Field implementation of the hybrid-ORS method demonstrates that the method can rapidly capture multiple profiles of the PM plumes and is well suited for improved quantification of fugitive PM EFs from vehicles traveling on unpaved roads.

Keywords: LIDAR; AP-42; PM_{10}; $PM_{2.5}$; Flux tower method.

INTRODUCTION

Concentrations of particulate matter (PM) with aerodynamic diameters ≤ 10 µm (PM_{10}) and ≤ 2.5 µm ($PM_{2.5}$) have positive correlations with the occurrence of human respiratory and cardiac illnesses (Dockery and Pope, 1994; Pope and Dockery, 2006). PM impairs visibility (Watson, 2002) and influences climate change by scattering and absorbing solar radiation (Storelvmo *et al.*, 2011). Fugitive PM refers to PM that is discharged to the atmosphere, but not in a confined flow stream (Watson and Chow, 2000; U.S. Environmental Protection Agency, EPA, 2011). Such is the case with fugitive PM emitted to the atmosphere when vehicles travel on unpaved surfaces. According to the 2011 U.S. National Emissions Inventory (NEI), of the primary combined natural and anthropogenic PM emissions to the atmosphere, fugitive emissions from all paved and unpaved roads were 54% and 23% of the PM_{10} and $PM_{2.5}$ emissions, respectively (U.S. EPA, 2015b). NEI estimates are based on PM mass emission factors (EFs) in U.S. EPA's AP-42 database and are rated as highly uncertain (U.S. EPA, 2015a). The high uncertainty reflects the nature of fugitive emission plumes that can: 1) have short lifetimes (often less than one minute) (McFarland *et al.*, 2007; Du *et al.*, 2013), 2) exist with large spatial scales (tens to hundreds of meters) (Du *et al.*, 2011a), 3) can travel aloft, and 4) be heterogeneous (McFarland *et al.*, 2007). There remains a need for improving the accuracy of fugitive PM EFs (Du *et al.*, 2011a) with measurement methods appropriate for the characteristics of fugitive PM plumes to improve national and global PM emission inventories.

Optical remote sensing (ORS) methods are well suited to quantify fugitive PM EFs because they allow real-time and in-situ monitoring of emissions and they measure multiple cross-sections of the plumes over a large range of length scales (tens to hundreds of meters) over time periods of tens of seconds. Thus, ORS methods have the potential to facilitate fast and cost-effective updating of EFs according to the needs of NEIs (NARSTO, 2005; Miller *et al.*, 2006). Another method used for estimating fugitive PM EFs is the

* Corresponding author.
Tel.: 1-217-333-6963; Fax: 1-217-333-9464
E-mail address: mrood@illinois.edu

flux tower method, where fugitive PM EFs are quantified with multiple point-measurements of PM mass concentrations, using optically-based instruments (i.e., DustTraks™). The instruments are located in vertical and horizontal arrays mounted on one or more towers (Gillies *et al.*, 2005; Kuhns *et al.*, 2010), so that multiple areas of the plume can be sampled simultaneously. As with other optical methods, to allow quantification of PM mass EFs, ORS measurements entail conversion of optical measurements into PM mass concentrations. This is typically achieved by quantifying the mass extinction efficiency (MEE) values of the PM, which is defined as the ratio of the measured light extinction to measured PM mass concentration.

Some fugitive PM mobile sources have been characterized previously by ORS methods. These include movement of vehicles on unpaved roads (Gillies *et al.*, 2005; Du *et al.*, 2011b), movement of helicopters over unpaved surface (Du *et al.*, 2011b), movement of agricultural tractors (Holmén *et al.*, 1998) and harvesters (Faulkner *et al.*, 2009), and open burning and detonation (Yuen *et al.*, 2014). Fugitive PM EFs of military and civilian vehicles have been compared using flux tower method, for vehicles traveling from 10 to 80 km/hr, and vehicle masses between 1 and 17 tonnes (Gillies *et al.*, 2005).

This paper describes a new hybrid-ORS method and its results from field implementation to measure fugitive PM EFs for PM_{10} and $PM_{2.5}$ for tracked and wheeled military vehicles traveling on unpaved roads in a desert region. The difference between the ORS method reported in Du *et al.* (2011a) and this hybrid-ORS method is in the way the MEE values for PM_{10} and $PM_{2.5}$ are determined. In the earlier ORS method, MEE values were determined by first determining particle size distributions (PSDs) using wavelength-dependent light extinction measurements obtained with an open path-laser transmissometer (OP-LT) and an open-path Fourier Transform Infrared spectrometer. Then, MEE values were calculated using PSDs and assumed particle density and refractive index using Mie-Lorenz theory (Varma *et al.*, 2006; Du *et al.*, 2011a). In the hybrid-ORS method reported here, MEE values are determined by simultaneously measuring real-time light extinction with an OP-LT and PM_{10} and $PM_{2.5}$ mass concentrations with optically based DustTrak™ monitors. This hybrid-ORS method offers more operational simplicity, since a PM mass concentration monitor is used that does not require assumptions pertaining to particle density or refractive index. The hybrid-ORS method also enables measurement across the entire plume cross-section. The EFs determined by this hybrid-ORS method are then compared to EFs derived from the flux tower method and AP-42 models. Current AP-42 EFs for vehicle movement on unpaved industrial roads have been based on consideration of vehicles used in a variety of industries such as surface mining and construction, and they correspond to vehicles with masses between 2 and 260 tonnes, traveling from 8 to 69 km/hr. These values encompass the characteristics of the vehicles studied here which traveled from 8 to 69 km/hr with masses between 12 and 64 tonnes (U.S. EPA, 2015a). EFs measured in this research may be used by facilities using vehicles that travel on unpaved roads with similar masses and modes of traction to assess the contribution of such vehicles to PM emissions and subsequently impacts of the operation of such vehicles on air quality. The method is also applicable to sources that produce fugitive PM plumes.

METHODS

EF Measurement with the Hybrid-ORS Method

EFs were determined by integrating two dimensional (2-D) PM mass concentration profiles during each plume event with wind speed, wind direction, and duration of each event (Eq. (1), Fig. 1):

$$\mathrm{EF} = \frac{1}{Y} \times \sum_{t=0}^{T} \left(\sum C_m(\Delta A, t) \Delta A \right) u(z) \cos\theta \Delta t \quad (\text{g-PM/km}) \tag{1}$$

where Y is the distance the vehicle traveled when the plume was measured during each plume event; T is total duration of the event; $C_m(\Delta A,\ t)$ is the 2-D mass concentration profile of PM_{10} or $PM_{2.5}$ in the plume at time, t, within the differential area ΔA (Fig. 2 (a)); $u(z)$ is the wind speed at the height z; and θ is the angle between the wind direction and the normal direction to the ORS observing plane during that event. Typical ranges of values for parameters in Eq. (1) are shown in Table 1. The integration of 2-D PM mass concentration profiles (Eq. (1)) was completed within the ORS observing plane using polar coordinates to define ΔA with a longitudinal resolution of 15 m and vertical dimension defined by the scanning angle and the respective radial distance (Fig. 2(a)). Values of $C_m(\Delta A,\ t)$ profiles for PM_{10} or $PM_{2.5}$ were determined from the 2-D light extinction profiles, and PM_{10} or $PM_{2.5}$ MEE values using Eq. (2):

$$C_m(\Delta A, t) = \frac{\sigma(\Delta A, t)}{\mathrm{MEE}} \tag{2}$$

where $\sigma(\Delta A,\ t)$ represents a 2-D extinction profile.

The 2-D light extinction profiles were determined from the range-resolved backscattered photon counts measured by the Micro-Pulse Light Detection and Ranging (LIDAR; MPL) instrument (SigmaSpace, MPL-4B-527). To determine the 2-D light extinction profiles, the MPL was mounted on a vertically scanning positioner (ORBIT, Advanced Technologies, AL-4011-1E with control system AL-1613-3J) and pointed perpendicular to the plume's path while scanning vertically through the plume (Fig. 2(b)). The region scanned by the MPL defines the ORS observing plane (Fig. 2(a)). The photon counts were measured as pulsed laser light emitted from the MPL and then backscattered by the plume's PM toward the MPL's detector. The photon counts were corrected, normalized and then converted to normalized relative backscatter (NRB) values (Campbell *et al.*, 2002). To convert the 2-D NRB profiles to 2-D light extinction profiles the near-end LIDAR inversion technique was used (Fernald *et al.*, 1972; Du *et al.*, 2011a) with a reflective target that was located so that the plume was between the MPL and the target. The MPL recorded photon counts at 1 Hz for the entire duration of each plume.

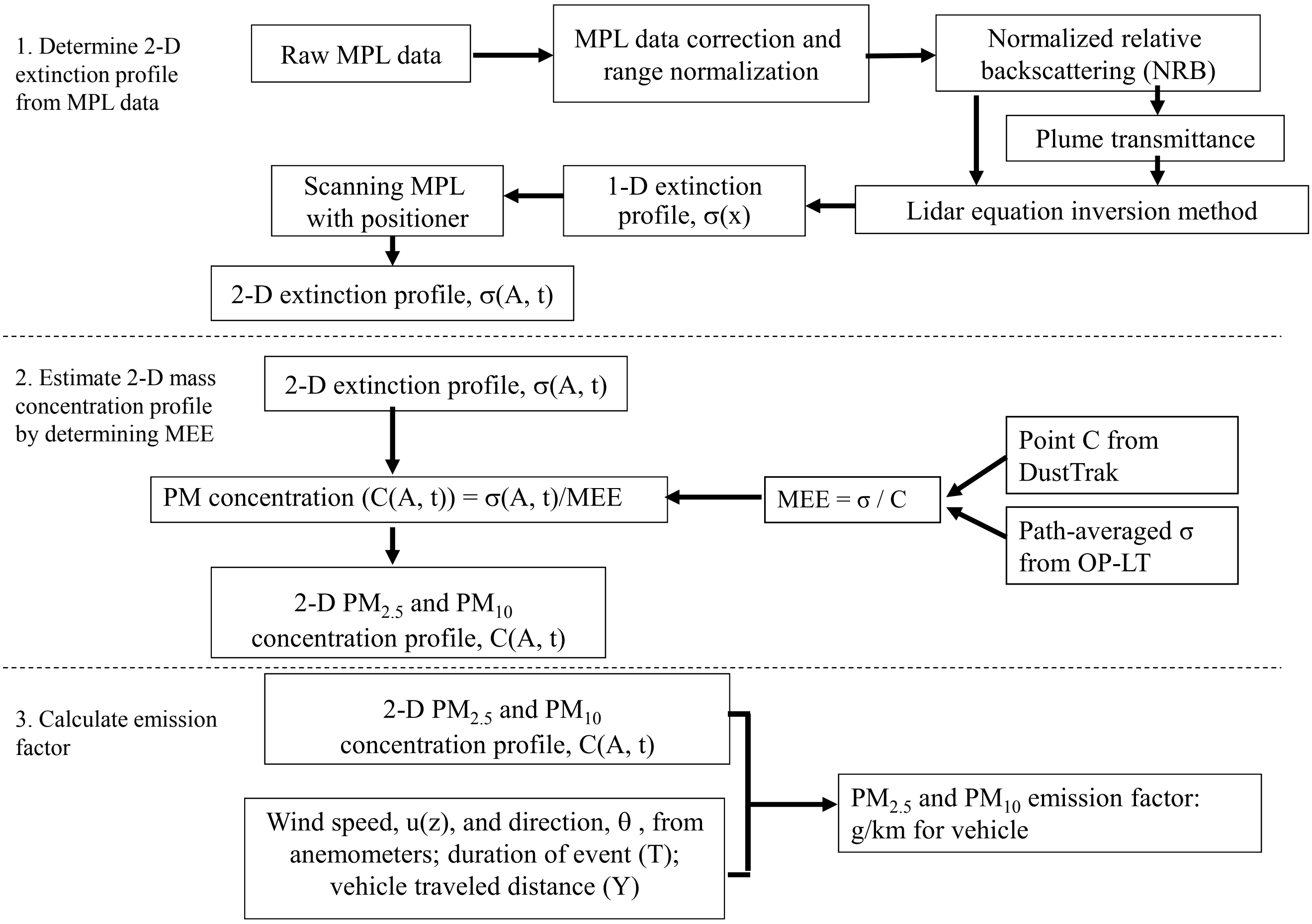

Fig. 1. Flow chart of method used to estimate mass emission factors for PM_{10} and $PM_{2.5}$ produced from the movement of vehicles on unpaved roads. Both MPL and OP-LT measure light extinction for total suspended particles (TSP), while DustTraks™ measure mass concentrations of PM_{10} or $PM_{2.5}$.

The MEE values for PM_{10} or $PM_{2.5}$ were determined from *in-situ path-integrated total light extinction* measurements divided by *in-situ PM_{10} or $PM_{2.5}$ point mass concentration* measurements, respectively. Light extinction was measured with a custom OP-LT (IMACC Inc.), at 1.7 m above ground that was co-located along the horizontal path of the MPL (Fig. 2(b)). The OP-LT used a modulated He-Ne laser operating at 1 Hz and transmitted light at 670 nm that was then reflected to the detector of the OP-LT by a custom retroreflector. These path-integrated light extinction values for the fugitive PM were determined by considering the signals detected by the OP-LT when a plume was and was not passing between the laser source and the retroreflector. PM_{10} and $PM_{2.5}$ mass concentrations were measured with calibrated light scattering DustTraks™ (Model 8520, TSI Inc.) at a rate of 1 Hz. The DustTraks™ were calibrated by comparing their light scattering measurements with gravimetric PM mass concentration measurements inside a dust resuspension chamber, for dust that was collected at the measurement site (Kuhns *et al.*, 2010). The DustTraks™ were located on three vertical towers. One tower contained DustTraks™ at five different heights that measured both PM_{10} and $PM_{2.5}$. The other two towers contained DustTraks™ at five different heights that measured only PM_{10} (Kuhns *et al.*, 2010). The average PM_{10} mass concentrations obtained at the lowest located DustTraks™ on all three towers and the $PM_{2.5}$ mass concentrations obtained at the lowest located DustTrak™ on one tower, all located at a height of 1.7 m, were used to calculate the PM_{10} and $PM_{2.5}$ MEE values, respectively. The lowest located DustTraks™ were used seeing they corresponded to the same height as the optical path of the OP-LT and they were co-located along the same path as the OP-LT, so the DustTraks™ and OP-LT sampled similar masses of PM. MEE values were then determined by dividing the *path-integrated and time-averaged total PM light extinction values* from the OP-LT by the *time-averaged PM_{10} or $PM_{2.5}$ mass concentrations* measured by the DustTraks™, for the duration of each plume (Hashmonay *et al.*, 2009). This method assumes that the averaged MEE values, describing the ratio of total PM light extinction to PM_{10} or $PM_{2.5}$ concentration, are representative of the PM plume within the scanning plane of the MPL during each emission event.

Use of the OP-LT required a wavelength correction in the MEE values because the OP-LT and MPL measurements occurred at 670 nm and 527 nm, respectively. The wavelength correction factor was determined by considering the PSD measured before, in a similar desert environment

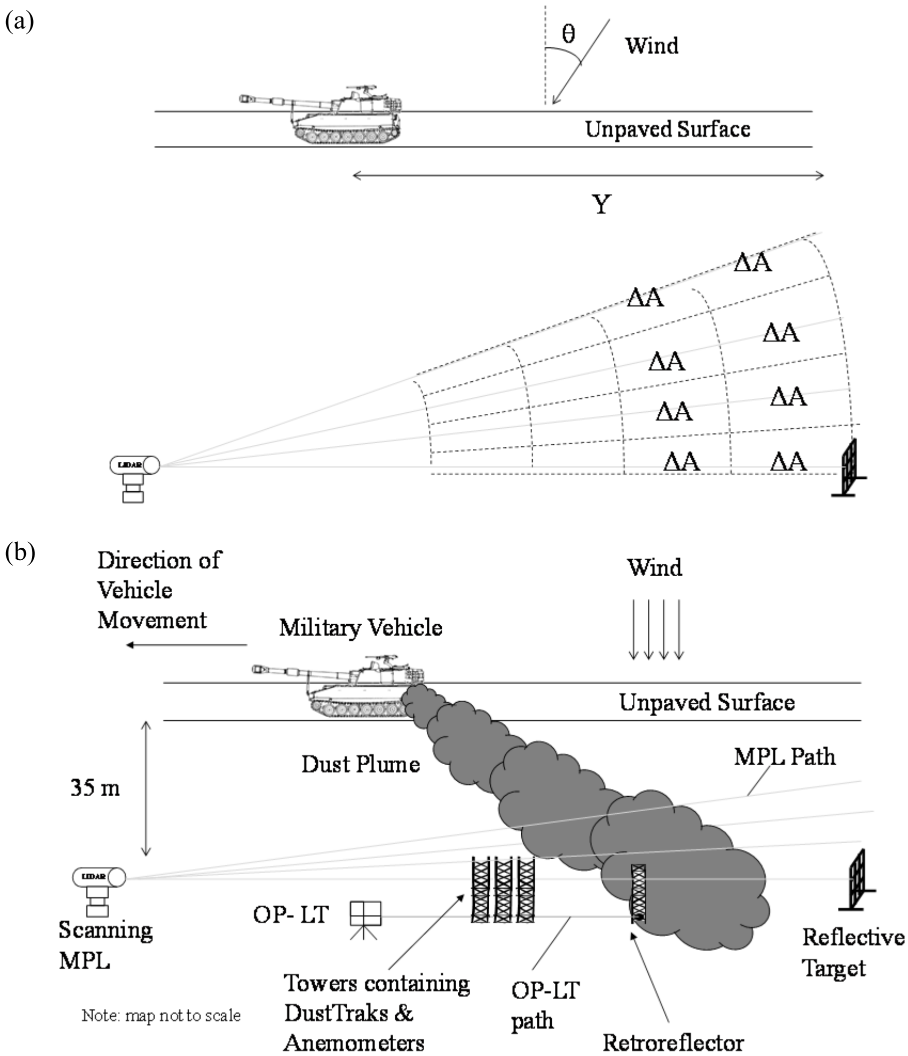

Fig. 2. (a) Parameters in Eq. (1) – θ: wind angle from perpendicular to plume, Y: vehicle travelling distance, and ΔA: differential plume area, where ΔA center points are 15 m (MPL resolution) apart. All ΔAs define the ORS scanning plane (outermost dotted lines), which is parallel to the road. (b) Source and instrument layout during the field campaign.

Table 1. Typical values in Eq. (1).

Parameter	Range
Vehicle travelling distance (Y, m)	Site 1: 258 to 341
	Site 2: 172 to 270
Wind speed at 1.87 m height ($u_{1.87}$, m/s)	1 to 4
Wind direction (θ,°)	5 to 55 from the line normal to the observing plane
Duration of event (T, s)	40 to 90
Differential area for EF integration (ΔA, m^2)	10 to 461

(Varma *et al.*, 2006; Du *et al.*, 2011a, b) and was varied by changing the mean diameter by number, so $PM_{2.5}/PM_{10}$ was varied. Mie-Lorenz theory (Bohren and Huffman, 1983) was then used to calculate a wavelength correction factor for each selected PSD, assuming particles are spherical and a refractive index of 1.54 + 0i, a value that is representative of mineral dust. Based on values from Kandler *et al.* (2007), Petzold *et al.*, (2009), Seinfeld *et al.* (2004), and Sokolik *et al.* (1993), the real part of refractive index ranges from 1.53 to 1.59, and imaginary part ranges from 0.3×10^{-3} to 9.0×10^{-3} for mineral dust. It was observed that the wavelength correction factor was linearly related to $PM_{2.5}/PM_{10}$. Linear regression resulted in the following wavelength correction factor $\sigma_{ext527}/\sigma_{ext670} = 0.74 \times (PM_{2.5}/PM_{10}) + 0.68$, $R^2 = 0.97$ for six data points, that was used to convert the extinction coefficient at 670 nm (σ_{ext670}) to the extinction coefficient at 527 nm (σ_{ext527}), which was used to calculate the MEE values. These MEE values of PM_{10} and $PM_{2.5}$ were combined with the MPL extinction coefficient measurements to obtain 2-D mass concentration profiles of PM_{10} and $PM_{2.5}$.

Wind speeds were determined with 2-D cup anemometers (Wind Sentry, R. M. Young) measured at five elevations (1.87, 2.80, 4.20, 6.65, and 9.34 m) and wind direction was determined with a wind vane placed at 9.34 m (Wind Sentry, R. M. Young). The anemometers and wind vane were co-located on the three towers with the DustTraks™. Power law regressions were fitted to the measured wind speed values to determine wind speed at the heights of the light extinction measurements (U.S. EPA, 2000). Wind direction was treated as a constant vertically for each plume event. Duration of each plume event was determined by the amount of time the plume passed through the vertical measurement plane detected by the MPL. The duration of a sampling event begins when the MPL first detects non-zero light extinction at the ground level scan. The duration ends when the MPL no longer detects non-zero light extinction at the ground level scan.

Field Site and Vehicle Information

The hybrid-ORS method was implemented during September 2008 at a desert continental site located at Fort Carson, CO, USA. The three types of tracked vehicles tested and their masses are: M88 (HERCULES, 63.5 tonne), M270 (MLRS, 24.9 tonne), and M577 (12.3 tonne). A wheeled vehicle, Heavy Expanded Mobility Tactical Truck (HEMTT, 20.0 tonne), was also tested. These vehicles traveled along unpaved roads parallel to the measurement plane and perpendicular to wind direction. Each vehicle travelled at speeds between 8 and 32 km/hr and at their maximum speed. A Global Positioning System (GPS) was placed in the vehicles to monitor vehicle position and speed.

Two unpaved roads were selected for the measurements to accommodate changes in wind direction during the field campaign. The optical paths of the ORS instruments were parallel to and 35 m downwind from either road (Fig. 2(b)). The setback distance between the MPL and the OP-LT was 185 m for Site 1 and 105 m for Site 2. The distance between the MPL and the MPL's reflective target was 790 m for Site 1 and 445 m for Site 2 to ensure the detected plumes were between the MPL and reflective target during each plume event. The MPL continuously scanned at Site 1 at angles: 0° (horizontal), 1.519°, 3.036°, and 4.045°, or 0°, 2.025°, 4.045°, and 6.054° depending on the plume elevations. The MPL continuously scanned at Site 2 at angles: 0°, 4.588°, 9.119°, and 12.080°. The duration of a vertical scan cycle was 10–14 s and the duration of plumes passing through the measurement plane of the MPL was between 40 s and 90 s, which resulted in three to nine 2-D extinction profiles per plume event.

The soil type at Site 1 and Site 2 was Heldt clay loam and Razor-Midway complex clayloam, respectively (Kuhns *et al.*, 2010). Soil moisture content was assumed to be 1%, consistent with dry weather during the campaign and previous research at desert sites where moisture content was < 1% (Kuhns *et al.*, 2010). These values were used as inputs for the AP-42 EF models (U.S. EPA, 2015a) to compare the AP-42 results with the measured values.

Quality Control Procedures in Data Analysis

Quality control procedures were performed to remove invalid data. A plume event was removed if any data (e.g., vehicle speed, MEE, and wind data) were missing. Plume events were also removed if any one of the following conditions occurs:

1) the wind did not direct the plume to the MPL's scanning plane due to sudden wind direction change (i.e., $\theta > 55°$) or low wind speed (i.e., < 1.0 m/s). Large θ or low wind speed will cause the plume to not travel through the MPL's scanning plane, thus the MPL does not capture the entire cross-section of the plume horizontally.

2) the largest angle of vertical scan was not high enough to capture the highest part of the plume. These were cases when non-zero light extinction was detected at the largest angle of vertical scan, indicating that the plume extended above the highest level the MPL could capture.

3) the MPL measured zero backscatter signals from the reflective target. This means that the plume is too opaque (< 1% light transmittance). High opacity results in high uncertainty in determining the light extinction profile.

Data Analysis

Results from the hybrid-ORS measurements were compared with those from the flux tower measurements reported by Kuhns *et al.* (2010) and estimated using AP-42 EFs. Mean Percentage Differences (MPDs) between the hybrid-ORS results and results from the flux tower method or AP-42 model for each vehicle were estimated by Eq. (3):

$$\mathrm{MPD} = \frac{1}{N}\sum_{i=1}^{N}\frac{\mathrm{EF}_{\mathrm{alt,i}} - \mathrm{EF}_{\mathrm{hORS,i}}}{\mathrm{EF}_{\mathrm{hORS,i}}}\times 100\% \quad (3)$$

In Eq. (3), EF_{alt} is the EF determined by a method/model alternative to the hybrid-ORS method (i.e., flux tower method or AP-42 model), EF_{hORS} is the EF determined by the hybrid-ORS method, i refers to the EF data point at a select vehicle type and speed, and N refers to total number of vehicle speeds tested for a particular vehicle. EFs determined by the flux tower method were linearly interpolated to the average vehicle speeds used with the hybrid-ORS method to allow comparison of EFs from the two methods, at the same vehicle speed range.

AP-42 model uses Eqs. (4) and (5) for industrial roads and publicly accessible roads, respectively (U.S. EPA, 2015a):

$$\mathrm{EF} = 281.9k\left(S/12\right)^{0.9}\left(W/2.721\right)^{0.45}\ \text{(g-PM/km)} \quad (4)$$

$$\mathrm{EF} = 281.9[k'\left(S/12\right)\left(V/48.3\right)^{0.5}\left(m/0.5\right)^{-0.2} - C]\ \text{(g-PM/km)} \quad (5)$$

where $k = 0.15$ for $PM_{2.5}$ and $k = 1.5$ for PM_{10}, S is silt content (32%, Kuhns *et al.*, 2010)), W is mean vehicle mass (tonne), $k' = 0.18$ for $PM_{2.5}$ and $k' = 1.8$ for PM_{10}, V is mean vehicle speed (km/hr), m is surface soil moisture content (% by mass), and C is PM mass EF due to vehicle exhaust, brake wear, and tire wear (g/km) (U.S. EPA, 2015a).

C is negligible compared to the fugitive PM emissions (< 1% of fugitive PM emissions, U.S. EPA, 2011). Note that the AP-42 model for industrial roads does not include vehicle speed but includes vehicle mass as a parameter, while the model for publicly accessible roads includes vehicle speed but does not include vehicle mass as a parameter. Moreover, the model for industrial roads applies to vehicles ranging from 1.8 to 260 tonnes and from 8 to 69 km/hr, while the model for publicly accessible roads applies to vehicles ranging from 1.4 to 2.7 tonnes and 16 to 88 km/hr. While the vehicle speeds used with the hybrid-ORS measurements were within the range of the speeds used for both models and the vehicle masses were within the range of the masses used for the industrial road model, the vehicle masses were between 4 and 23 times larger than the range of masses used for the publicly accessible road model. Both AP-42 models also only consider vehicles that have four or more wheels (U.S. EPA, 2015a). However, three out of four vehicles used in this research are tracked vehicles. For the above reasons, discrepancies between results from the hybrid-ORS method and AP-42 models may exist.

RESULTS AND DISCUSSION

A series of the resulting 2-D PM_{10} mass concentration profiles is shown in Fig. 3 to provide graphical insight about the length and time scales of a fugitive PM event caused by a HEMTT vehicle traveling at 24 km/hr on an unpaved road. EF statistics for PM_{10} and $PM_{2.5}$ determined by the hybrid-ORS method versus vehicle speed are presented in Figs. 4 and 5, respectively. The EF data were first classified into vehicle speed ranges. The means and standard deviations of EF data within the same speed range were then calculated and plotted as data points and vertical lines, respectively. The EFs for tracked vehicles ranged from 206 g/km to 1,738 g/km for PM_{10} and from 78 g/km to 684 g/km for $PM_{2.5}$, depending on vehicle speed and vehicle type. The EFs for the wheeled vehicle ranged from 223 g/km to 4,339 g/km for PM_{10} and from 44 g/km to 1,627 g/km for $PM_{2.5}$.

Linear, quadratic, and power law regressions were completed to fit the data for each vehicle type. The power law regression resulted in the largest mean correlation coefficients (R^2). AP-42 models also fit parameters using the power law (U.S. EPA, 2015a), thus comparison of results from the hybrid-ORS and from AP-42 is facilitated by using the same model. Power law regressions of PM EFs obtained with the hybrid-ORS method are provided as a function of vehicle type and speed in Table 2.

For both PM_{10} and $PM_{2.5}$, we compared normalized EFs versus vehicle speed for four vehicles measured in this field campaign to facilitate comparison of results with Gillies *et al.* (2005). To obtain normalized EFs, the ratios of EFs at select speeds to the EF at maximum speed are calculated for each vehicle (Fig. 6). Linear fits were forced through the origin. A t-test was also performed to examine if the slopes for tracked and wheeled vehicles are significantly different (sample sizes and t-test results are shown in Table 3). R^2 values for the linear regressions of the normalized PM_{10} EFs versus vehicle speed are larger than the normalized $PM_{2.5}$ EFs versus vehicle speed, especially for tracked vehicles. The slopes of the linear fits for the wheeled vehicle's normalized PM_{10} EFs versus vehicle speed support the result by Gillies *et al.* (2005), where results by both us and Gillies *et al.* are 0.014. The t-test shows that the slopes for tracked and wheeled vehicles are not significantly different from each other at 95% confidence level for both PM_{10} and $PM_{2.5}$ (p-values > 0.94 > 0.05).

The relationship between the slope of PM_{10} and $PM_{2.5}$ EF versus vehicle speed [(g/km)/(km/hr)] and the vehicle's mass (kg) were also examined and shown in Fig. 7. To obtain the slope of PM EF versus vehicle speed, linear regression between each vehicle's PM EF versus speed is obtained. The slopes of PM_{10} EF versus vehicle speed from Gillies *et al.* (2005) are also added in Fig. 7 for comparison. Our results show that the slopes of PM_{10} and $PM_{2.5}$ EF versus vehicle speed are independent of vehicle masses for tracked vehicles. Linear regression significance tests of the results from the hybrid-ORS method show that p-values for PM_{10} and $PM_{2.5}$ are 0.57 and 0.31, respectively, for the three tracked vehicles. Hence, there is not a statistically significant linear relationship between the slopes of PM EF versus vehicle speed and the vehicle masses at 95% confidence level. These results are in contrast to the results by Gillies *et al.* (2005), where a strong linear relationship for wheeled vehicles was observed, with slope of PM EF versus vehicle speed [(g/km)/(kg km/hr)] = 3 × vehicle masses (tonne), $R^2 = 0.95$, for nine vehicles with masses between 1 and 18 tonnes. A possible explanation is that there may be an upper limit of road surface material that is available for resuspension, so further increase in vehicle mass does not necessarily increase the PM EF per unit speed. Our tested vehicles have larger masses than vehicles tested in Gillies *et al.* (2005), so it is possible that vehicles tested in Gillies *et al.* (2005) do not resuspend the maximum amount of road surface material, thus explaining the linear relationship reported by Gillies *et al.* (2005). The slope of PM_{10} EF of HEMTT versus speed is 62.2 (g/km)/(km/hr), while the slope of the same vehicle by Gillies *et al.* (2005) is 50 (g/km)/(km/hr).

Comparison of Results from Hybrid-ORS Method to Concurrent Flux Tower Method

Results from the hybrid-ORS and flux tower methods are compared and the results of EF versus vehicle speed are shown in Fig. 4 for PM_{10} and in Fig. 5 for $PM_{2.5}$. MPD values for EFs from hybrid-ORS and flux tower EFs for all four vehicles are shown in Table 4, which range from –25% to 40% for PM_{10}. There are no variances reported from the flux tower method to statistically test the difference between the hybrid-ORS and flux tower methods. EFs for $PM_{2.5}$ from the flux tower method are not available.

In addition, results from the hybrid-ORS and flux tower methods for PM_{10} EF versus tracked vehicle momentum are compared and shown in Fig. 8. Kuhns *et al.* (2010) calculated the mean ratios of PM_{10} EF to vehicle momentum for tracked and wheeled vehicles at each site. We performed similar calculations and compared our results to Kuhns *et al.* (2010) in Table 5. The 95% confidence intervals for our results and Kuhns *et al.* results were also compared. For

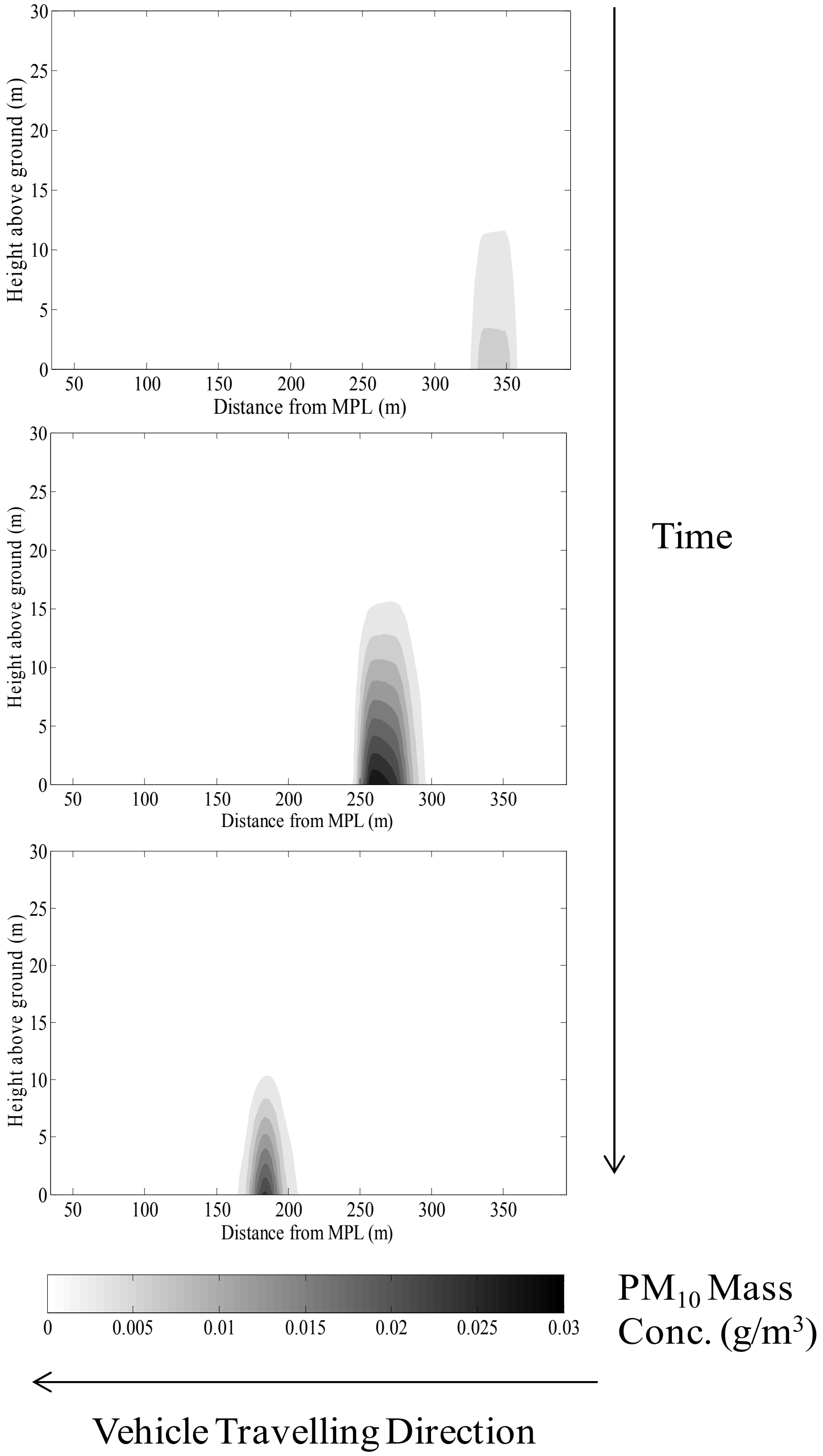

Fig. 3. Example of evolution of PM_{10} mass concentration profiles when a HEMTT vehicle passed at the speed of 24 km/hr, as it moves along a line parallel to the MPL observation plane and towards the MPL. The time elapsed between two consecutive profiles is 14 s.

tracked vehicles, the confidence intervals for both data sets did not overlap, meaning that the differences between these data sets are significant at 95% confidence level. The mean ratio of our data (0.004 (g PM_{10}/km)/(kg m/s)) is smaller than the mean ratio of data from Kuhns *et al.* (0.006 (g PM_{10}/km)/(kg m/s)) at Site 1, and larger (0.009 (g PM_{10}/km)/(kg m/s)) than data from Kuhns *et al.* (0.004 (g PM_{10}/km)/(kg m/s)) at Site 2. For wheeled vehicles, the

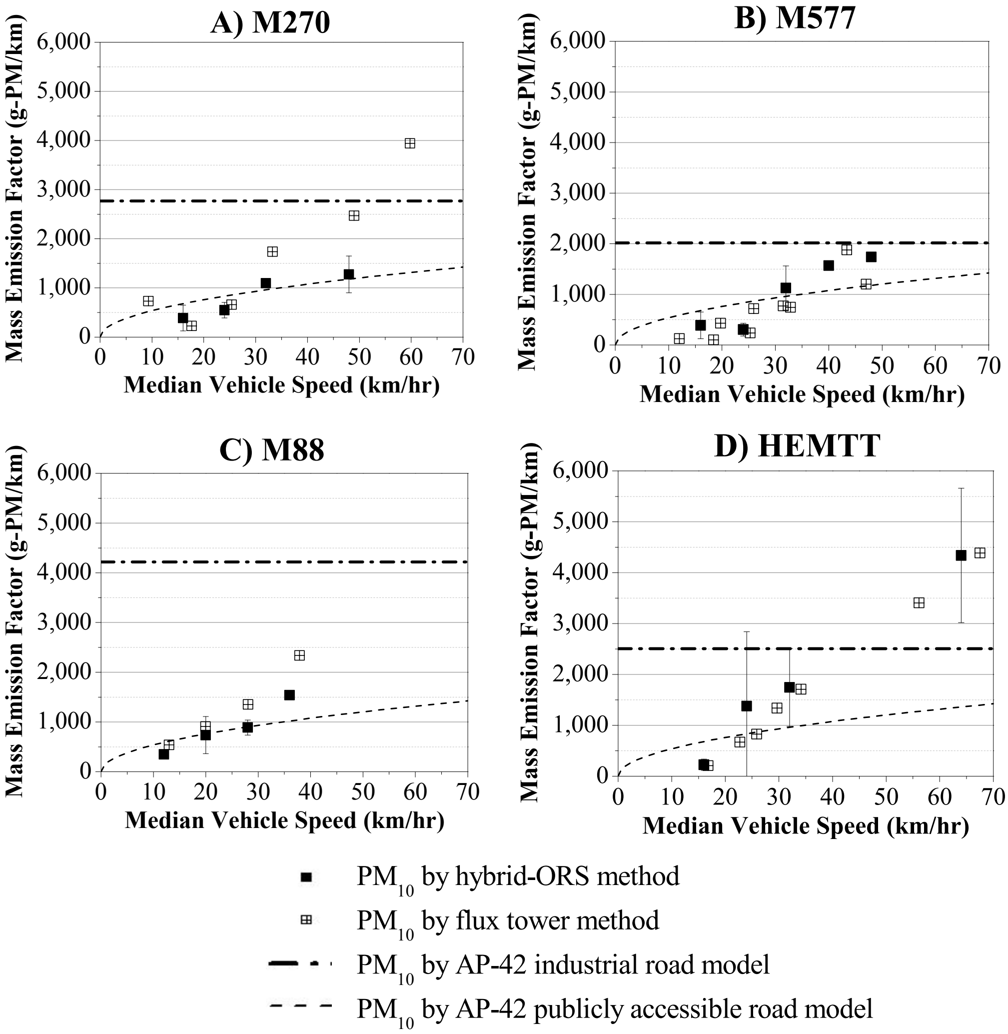

Fig. 4. Comparison of measured PM_{10} mass emission factors by hybrid-ORS and flux tower methods (Kuhns *et al.*, 2010) and modeled PM_{10} emission factors from AP-42 industrial road model and publicly accessible road model.

confidence intervals overlapped, meaning that the differences between the data sets are insignificant at 95% confidence. From the above results, there is no strong evidence to support whether the flux tower EFs are generally larger or smaller than hybrid-ORS EFs. The two methods have inherent differences. The flux tower method provides PM mass concentrations measured with the light scattering based DustTraks™ that are mounted on towers to detect the cross-sections of the plumes. The hybrid-ORS method detects PM mass concentration by inferring light extinction measured by an MPL range-resolved laser beam that scans the plumes' vertical cross-sections. The time resolution of the DustTraks™ used with the flux tower method and the hybrid-ORS is 1 Hz, whereas it takes 10–14 s for the ORS to complete a vertical scan. Moreover, ORS requires a longer setback distance from the area of measurement to measure taller plumes, which increases the area required to perform the ORS measurements. The ORS also requires a downwind distance so that the plume can disperse to the ORS scanning plane, but such distance introduces particle loss due to deposition. Such particle loss is believed to be insignificant. An earlier field campaign showed that PM_{10} loss is not measurable at a downwind distance of 100 m. Such results have also been compared with ISC3 model that only 4.3% of PM_{10} is removed at a downwind distance of 100 m (Etyemezian *et al.*, 2004). Both methods have been shown applicable for the measurement of fugitive PM emissions factors. Further validation and method uncertainty quantification can be achieved under controlled environmental conditions (such as choosing a location with low variations of wind speed and direction during the experiment) and with use of known emissions (such as by means of using a high volume dust generator). Such experiments in the ambient are rare due to cost considerations but they are valuable for future implementation of novel measurement methods.

Comparison of Results from Hybrid-ORS Method to AP-42 Model

PM_{10} and $PM_{2.5}$ EFs determined by the hybrid-ORS method were also compared with results from the AP-42 EFs for vehicles traveling on unpaved industrial and publicly accessible roads (Figs. 4 and 5 for PM_{10} and

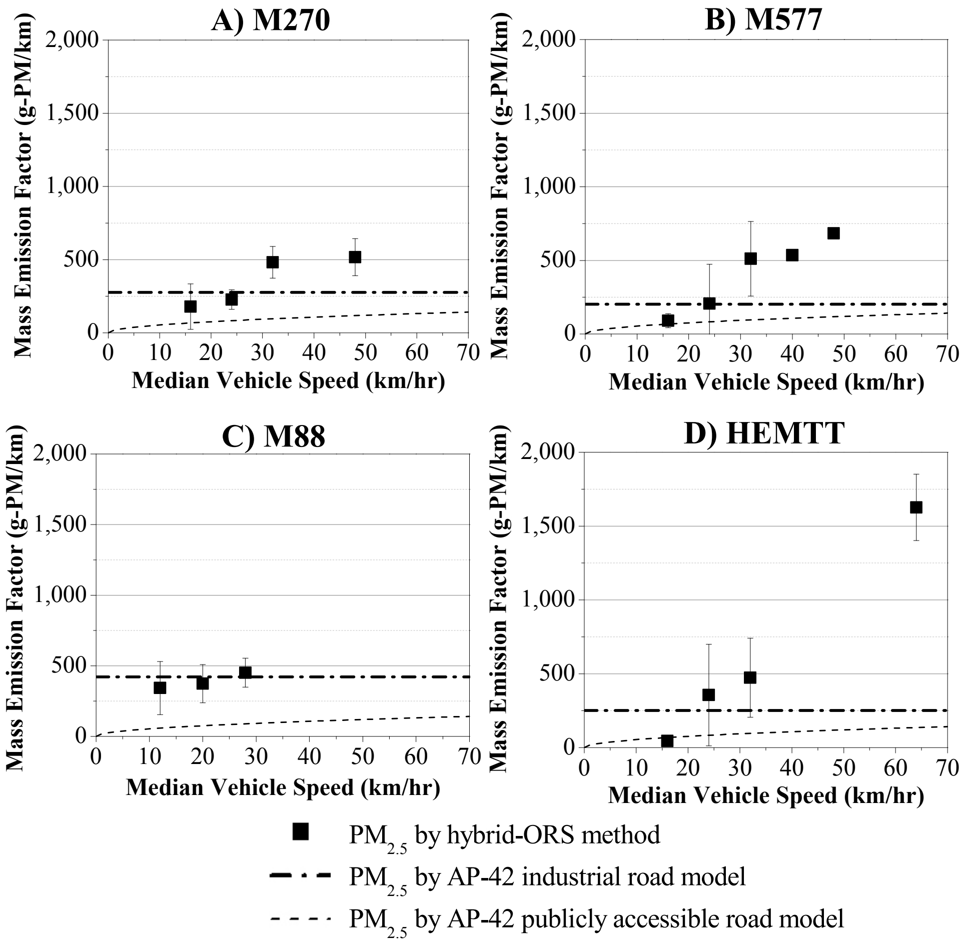

Fig. 5. Comparison of measured $PM_{2.5}$ mass emission factors by hybrid-ORS method and modeled emission factors from AP-42 industrial road and publicly accessible road models.

Table 2. Power law regressions of PM mass emission factors as a function of speed for select vehicles.

Vehicle (traction)	Particle size range	Regression [a]	R^2	Number of tested speeds	Number of events
M270 (tracked)	PM_{10}	$EF = 15v^{1.17}$	0.92	4	13
	$PM_{2.5}$	$EF = 9v^{1.07}$	0.87		
M577 (tracked)	PM_{10}	$EF = 2.87\ v^{1.66}$	0.79	5	21
	$PM_{2.5}$	$EF = 0.51v^{1.90}$	0.95		
M88 (tracked)	PM_{10}	$EF = 15v^{1.28}$	0.97	4	14
	$PM_{2.5}$	$EF = 155v^{0.31}$	0.89		
HEMTT (wheeled)	PM_{10}	$EF = 1.49v^{1.98}$	0.86	4	15
	$PM_{2.5}$	$EF = 0.09v^{2.42}$	0.89		

[a] EF = PM mass emission factor (g/km), v = vehicle speed (km/hr).

$PM_{2.5}$, respectively). Since AP-42 industrial road model is independent of vehicle speed (Eq. (4)), the lines for this model are horizontal. AP-42 publicly accessible road model, however, depends on vehicle speed (Eq. (5)), so the lines for this model are curved. MPDs between hybrid-ORS results and AP-42 industrial and publicly accessible roads modeled values for each vehicle are shown in Table 4. The MPDs between the EFs estimated by the hybrid-ORS method and those modeled by AP-42 for industrial roads for all test conditions range from 222% to 535% for PM_{10}, and from –14% to 76% for $PM_{2.5}$. The MPDs between EFs measured by the hybrid-ORS method and modeled by AP-42 for publicly accessible roads for all test conditions range from 10% to 34% for PM_{10} and from –81% to –49% for $PM_{2.5}$.

MPD values show that PM_{10} EFs provided by the AP-42 model for the industrial road were generally larger than EFs derived from the hybrid-ORS method. A similar trend was also reported regarding comparison between the flux tower method and the AP-42 model (Gillies *et al.*, 2005; Kuhns *et al.*, 2010). The AP-42 model for publicly accessible

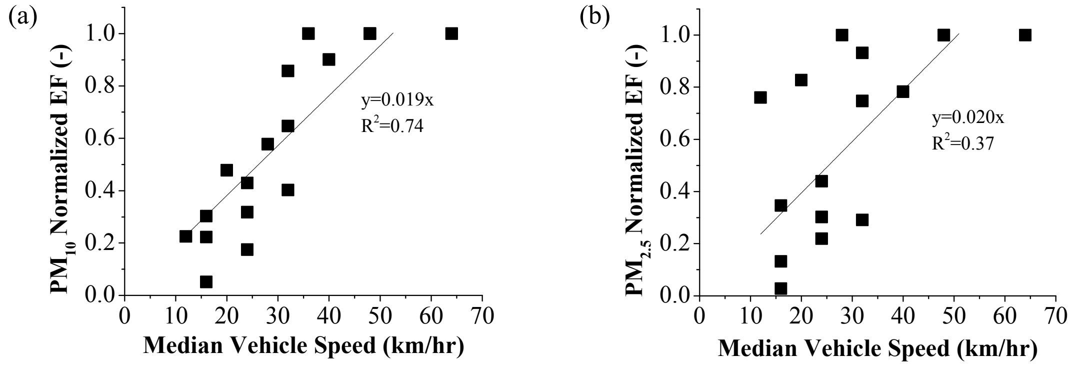

Fig. 6. Linear regression plots of (a) PM_{10} and (b) $PM_{2.5}$ normalized EFs (unitless) against vehicle speeds (km/hr) for the four vehicles measured in our field campaign. Normalized EF is defined as the ratio of EF at a specified vehicle speed to EF measured at the maximum speed for each vehicle.

Table 3. Linear regression statistics of PM_{10} and $PM_{2.5}$ normalized EFs against vehicle speeds. Zero intercept was set for the linear regressions. Normalized EFs are the ratio of the EF to the EF at maximum speed for each vehicle. The p-values indicate that there is no significant difference between the slopes of tracked and wheeled vehicles for PM_{10} and $PM_{2.5}$ at 95% confidence level.

Vehicle Type	Normalized PM_{10} EF (-)			Normalized $PM_{2.5}$ EF (-)		
	Slope	R^2	Number of data	Slope	R^2	Number of data
Four vehicles combined [a]	0.019	0.74	16	0.020	0.37	15
Three tracked vehicles	0.021	0.81	12	0.023	0.31	11
One wheeled vehicle	0.014	0.91	4	0.013	0.84	4
p-value		0.94			0.95	
Nine wheeled vehicles [b]	0.014	0.77	36			

[a] Four vehicles are: M270 (tracked), M577 (tracked), M88 (tracked), and HEMTT (wheeled).
[b] Nine wheeled vehicles are: Dodge Neon, Dodge Caravan, Ford Taurus, GMC G20 van, HMMWV, GMC C5500, HEMTT, M923A2, and M1078 LMTV (Gillies *et al.*, 2005).

road tends to underestimate $PM_{2.5}$ EFs when compared to the hybrid-ORS method. The underestimations may result because the masses of the tested vehicles during this field campaign were between 4 and 23 times higher than the upper mass limit for which the AP-42 model for publicly accessible road should be applied. This puts into perspective the high uncertainty associated with the existing AP-42 EFs, and indicates that possibly silt content and surface soil moisture in the current AP-42 EF equations do not fully capture the variability of PM EFs generated from vehicles travelling on unpaved surfaces.

Sensitivity Analysis of Wavelength Corrections of MEE Values Due to Particle Properties

A sensitivity analysis was performed to examine the influence of refractive index and PSD on the wavelength corrections of MEE values. As the base case, we used refractive indices of 1.53–4.2 × 10^{-3}i for 527 nm (MPL) and 1.53–6.6 × 10^{-3}i for 670 nm (OP-LT) (Hess *et al.*, 1998), PSD based on number concentrations (geometric mean diameter = 0.6 µm and geometric standard deviation = 1.8), and particle density of 2.6 g/cm^3 for mineral dust (Hess *et al.*, 1998) to calculate the PM_{10} and $PM_{2.5}$ MEEs for both wavelengths. As mentioned above, the real part of refractive index ranges from 1.53 to 1.59, and imaginary part ranges from 0.3 × 10^{-3} to 9.0 × 10^{-3} for mineral dust. A previous sensitivity analysis studied MEE values when the real and imaginary parts of the refractive index were varied from 1.35 to 1.60 and 0 to 0.01, respectively, and observed that MEE values ranged from 0.33 to 0.35 m^2/g (percent difference < 6%) (Du, 2007). Realizing that the imaginary part of the refractive index does not change MEE values substantially, MEE calculations in this sensitivity analysis were repeated by using only the real part of the refractive index values of 1.50, 1.53, and 1.60. PSDs were also varied by changing the mean number-based particle diameter from 0.4 to 0.7 µm and geometric standard deviation from 1.75 to 1.90. The chosen ranges are based on PSD data of desert dust obtained during a field campaign in Yuma, AZ (Du *et al.*, 2011b). Particle diameter was integrated from 0.05 µm to 40 µm to calculate total PM extinction coefficients with the use of Mie-Lorenz Theory, and was integrated from 0.05 µm to 10 µm or from 0.05 µm to 2.5 µm to calculate PM_{10} or $PM_{2.5}$ mass concentration, respectively. MEE values at MPL and OP-LT wavelengths were then calculated from the total PM extinction coefficients and PM_{10} or $PM_{2.5}$ mass concentration. The wavelength correction factor was calculated by taking the ratios of OP-LT to MPL derived MEE values.

The wavelength correction factors are between 0.971 and 1.081 for the ranges of PSDs and refractive indices evaluated (Table 6). By varying the geometric mean diameters and standard deviations of PSDs from the base case, the wavelength correction factor varied < 5%. Therefore, the correction in MEE values due to wavelength difference between the OP-LT and MPL is not sensitive to either PSD or real refractive index for conditions experienced during the field campaign.

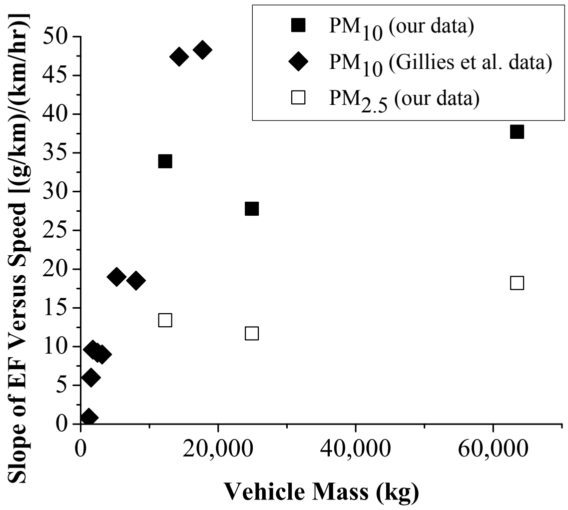

Fig. 7. Relationship between the slope of PM EF versus vehicle speed ((g/km)/(km/hr)) and vehicle mass (kg). Our data have three data points representing three tracked vehicles. Gillies *et al.* (2005) data have nine data points representing nine wheeled vehicles.

Table 4. Mean Percentage Differences (MPD) between hybrid-ORS emission factor results to corresponding results from the flux tower and AP-42 results for industrial roads and publicly accessible roads for each vehicle type. Flux tower measurements for $PM_{2.5}$ are unavailable.

Site location and vehicle type		Flux tower measurement	AP-42 emission factor model for industrial road		AP-42 emission factor model for publicly accessible road	
Site no.	Vehicle type	MPD[a] for PM_{10} (%)	MPD[a] for PM_{10} (%)	MPD[a] for $PM_{2.5}$ (%)	MPD[a] for PM_{10} (%)	MPD[a] for $PM_{2.5}$ (%)
1	M270	31	324	–3	27	–71
1	M88	40	535	10	10	–81
2	M577	–22	222	–14	34	–66
2	HEMTT	–25	277	76	13	–49

[a] MPD = mean percent difference (Eq. (3)).

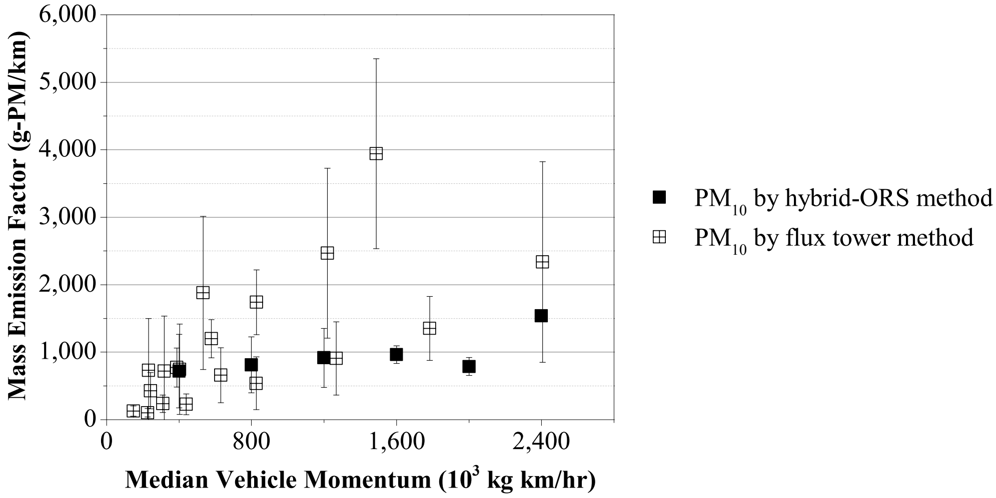

Fig. 8. Comparison of hybrid-ORS and flux tower PM_{10} mass emission factors versus vehicle momentum for tracked vehicles.

Table 5. Comparison of PM_{10} EFs that are normalized to their momentum for tracked and wheeled vehicles between our data and Kuhns *et al.* (2010) data. Values are presented as the ratios ± uncertainty, which are standard deviations. Numbers in parentheses represent number of samples. Numbers in brackets show the corresponding 95% confidence intervals.

	PM_{10} EF/ vehicle momentum [(g PM_{10}/km)/(kg m/s)]	
	Our data	Kuhns *et al.*, 2010
Site 1 Tracked	0.004 ± 0.003 (38) [0.003, 0.005]	0.006 ± 0.002 (157) [0.006, 0.006]
Site 2 Tracked	0.009 ± 0.004 (9) [0.007, 0.012]	0.004 ± 0.004 (34) [0.003, 0.005]
Site 2 Wheeled	0.009 ± 0.007 (15) [0.005, 0.013]	0.008 ± 0.003 (52) [0.007, 0.009]

Table 6. Sensitivity analysis of mass extinction efficiency (MEE) correction factors, described by the ratio of MEE values at red (670 nm) to green (527 nm) wavelengths, for three real parts of the refractive indices. In table a) the geometric standard deviation (GSD) is 1.8 and the mean diameters range from 0.4 to 0.7 µm. In table b) the mean diameter is 0.5 µm and the GSDs range from 1.75 to 1.90.

a) Geometric standard deviation = 1.8

Real part of refractive index	Mean diameter (µm)							
	0.4		0.5		0.6		0.7	
	MEE red to green wavelength correction factor for $PM_{2.5}$ or PM_{10}							
	$PM_{2.5}$	PM_{10}	$PM_{2.5}$	PM_{10}	$PM_{2.5}$	PM_{10}	$PM_{2.5}$	PM_{10}
1.50	0.971	0.972	1.022	1.021	1.051	1.051	1.066	1.066
1.53	0.988	0.988	1.036	1.037	1.065	1.065	1.081	1.080
1.60	1.005	1.004	1.038	1.037	1.050	1.050	1.050	1.050

b) Mean diameter = 0.5 µm

Real part of refractive index	Geometric standard deviation							
	1.75		1.80		1.85		1.90	
	MEE red to green wavelength correction factor for $PM_{2.5}$ or PM_{10}							
	$PM_{2.5}$	PM_{10}	$PM_{2.5}$	PM_{10}	$PM_{2.5}$	PM_{10}	$PM_{2.5}$	PM_{10}
1.50	1.015	1.015	1.022	1.021	1.027	1.027	1.031	1.031
1.53	1.031	1.031	1.036	1.037	1.042	1.042	1.047	1.046
1.60	1.039	1.038	1.038	1.037	1.037	1.037	1.035	1.036

CONCLUSIONS

Emission Factors (EFs) for fugitive PM_{10} and $PM_{2.5}$ emitted by vehicles travelling on desert unpaved roads were measured using a hybrid-optical remote sensing (ORS) method. This ORS method uses a micro-pulse lidar (MPL) to obtain vertically scanned 2-D extinction profiles. These extinction profiles were combined with mass extinction efficiency (MEE) values obtained from point PM_{10} and $PM_{2.5}$ mass concentrations and path-integrated open path-laser transmissometer (OP-LT) measurements to determine 2-D PM_{10} and $PM_{2.5}$ mass concentration profiles across each plume. EFs for fugitive PM_{10} and $PM_{2.5}$ were obtained by integrating 2-D mass concentration profiles with wind data and duration of each event. The EFs for tracked vehicles ranged from 206 g/km to 1,738 g/km for PM_{10} and from 78 g/km to 684 g/km for $PM_{2.5}$, depending on vehicle speed and vehicle type. The EFs for the wheeled vehicle ranged from 223 g/km to 4,339 g/km for PM_{10} and from 44 g/km to 1,627 g/km for $PM_{2.5}$. These PM EF results may be used by facilities to determine the impact of the operation of these vehicles on air quality impacted by fugitive dust.

EFs measured by hybrid-ORS method were compared with concurrent measurements of EFs using the flux tower method and EFs estimates by U.S. EPA AP-42 models. Mean percent differences (MPDs) between –25% and 40% were observed between the hybrid-ORS and flux tower methods for PM_{10}, which shows that there is no strong evidence to support whether the flux tower EFs are generally larger or smaller than hybrid-ORS EFs. Comparisons with AP-42 PM_{10} EFs resulted in MPD values between 222% and 535% for the industrial road case and between 10% and 34% for the publicly accessible road case. For $PM_{2.5}$, MPD values ranged between –14% and 76% for the AP-42 industrial road case and between –81% and –49% for the publicly accessible road case. These comparisons between hybrid-ORS and AP-42 EFs show that PM_{10} EFs estimated by the AP-42 model for industrial road were generally larger than EFs derived from the hybrid-ORS method. $PM_{2.5}$ EFs estimated by the AP-42 model for publicly accessible roads were generally smaller than EFs derived from the hybrid-ORS method.

Field implementation of the hybrid-ORS method shows that this method is well suited for quantifying fugitive PM EFs. The method offers the advantage of completely scanning multiple plume cross-sections during entire events and allowing for complete detection for tall or aloft plumes. Application of the method for sources of fugitive PM with different characteristics has the potential to expand the scope of current AP-42 EFs and increase their accuracy.

ACKNOWLEDGMENTS

The authors thank the support from Department of Defense (DoD) Project SI-1400 and Chinese Academy of Sciences Visiting Professorship for Senior International Scientists, Grant 2011T2Z17.The authors also thank DRI for providing global positioning system, DustTrak™, anemometer, and wind vane data.

REFERENCES

Bohren, C.F. and Huffman, D.R. (1983). *Absorption and Scattering of Light by Small Particles*, Wiley, New York.

Campbell, J.R., Hlavka, D.L., Welton, E.J., Flynn, C.J., Turner, D.D., Spinhirne, J.D., Scott, V.S. and Hwang, I.H. (2002). Full-Time, Eye-Safe Cloud and Aerosol Lidar Observation at Atmospheric Radiation Measurement Program Sites: Instruments and Data Processing. *J. Atmos. Oceanic Technol.* 19: 431–442.

Dockery, D.W. and Pope, C.A. (1994). Acute Respiratory Effects of Particulate Air Pollution. *Annu. Rev. Publ. Health* 15: 107–132.

Du, K. (2007). *Optical Remote Sensing of Airborne Particulate Matter to Quantify Opacity and Mass Emissions*, University of Illinois, p.133.

Du, K., Rood, M.J., Welton, E.J., Varma, R.M., Hashmonay, R.A., Kim, B.J. and Kemme, M.R. (2011a). Optical Remote Sensing to Quantify Fugitive Particulate Mass Emissions from Stationary Short-term and Mobile Continuous Sources: Part I. Method and Examples. *Environ. Sci. Technol.* 45: 658–65.

Du, K., Yuen, W., Wang, W., Rood, M.J., Varma, R.M., Hashmonay, R.A., Kim, B.J. and Kemme, M.R. (2011b). Optical Remote Sensing to Quantify Fugitive Particulate Mass Emissions From Stationary Short-Term and Mobile Continuous Sources : Part II. Field Applications. *Environ. Sci. Technol.* 45: 666–672.

Du, K., Shi, P., Rood, M.J., Wang, K., Wang, Y. and Varma, R.M. (2013). Digital Optical Method to Quantify the Visual Opacity of Fugitive Plumes. *Atmos. Environ.* 77: 983–989.

Etyemezian, V., Ahonen, S., Nikolic, D., Gillies, J., Kuhns, H., Gillette, D. and Veranth, J. (2004). Deposition And Removal of Fugitive Dust in the Arid Southwestern United States: Measurements and Model Results. *J. Air Waste Manage. Assoc.* 54: 1099–111.

Faulkner, W.B., Goodrich, L.B., Botlaguduru, V.S.V., Capareda, S.C. and Parnell, C.B. (2009). Particulate Matter Emission Factors for Almond Harvest as a Function of Harvester Speed. *J. Air Waste Manage. Assoc.* 59: 943–949.

Fernald, F.G., Herman, B.M. and Reagan, J.A. (1972). Determination of Aerosol Height Distributions by Lidar. *J. Appl. Meteorol.* 11: 482–489.

Gillies, J.A., Etyemezian, V. and Kuhns, H. (2005). Effect of Vehicle Characteristics on Unpaved Road Dust Emissions. *Atmos. Environ.* 39: 2341–2347.

Hashmonay, R.A., Kagann, R.H., Rood, M.J., Kim, B.J., Kemme, M.R. and Gillies, J. (2009). An Advanced Test Method for Measuring Fugitive Dust Emissions Using a Hybrid System of Optical Remote Sensing and Point Monitor Techniques. In *Atmospheric and Biological Environmental Monitoring*, Kim,Y.J., Platt, U., Gu, M.B. and Iwahashi, H. (Eds),. Springer Netherlands, pp. 73–81.

Hess, M., Koepke, P. and Schult, I. (1998). Optical Properties of Aerosols and Clouds: The Software Package OPAC. *Bull. Am. Meteorol. Soc.* 79: 831–844.

Holmén, B.A., Eichinger, W.E. and Flocchini, R.G. (1998). Application of Elastic Lidar to PM_{10} Emissions from Agricultural Nonpoint Sources. *Environ. Sci. Technol.* 32: 3068–3076.

Kandler, K., Benker, N., Bundke, U., Cuevas, E., Ebert, M., Knippertz, P., Rodríguez, S., Schütz, L. and Weinbruch, S. (2007). Chemical Composition and Complex Refractive Index of Saharan Mineral Dust at Izaña, Tenerife (Spain) Derived by Electron Microscopy. *Atmos. Environ.* 41: 8058–8074.

Kuhns, H., Gillies, J., Etyemezian, V., Nikolich, G., King, J., Zhu, D., Uppapalli, S., Engelbrecht, J. and Kohl, S. (2010). Effect of Soil Type and Momentum on Unpaved Road Particulate Matter Emissions from Wheeled and Tracked Vehicles. *Aerosol Sci. Technol.* 44: 187–196.

McFarland, M.J., Olivas, A.C., Atkins, S.G., Kennedy, R.L. and Patel, K. (2007). Fugitive Emissions Opacity Determination Using the Digital Opacity Compliance System (DOCS). *J. Air Waste Manage. Assoc.* 57: 1317–1325.

Miller, C.A., Hidy, G., Hales, J., Kolb, C.E., Werner, A.S., Haneke, B., Parrish, D., Frey, H.C., Rojas-Bracho, L., Deslauriers, M., Pennell, B. and Mobley, J.D. (2006). Air Emission Inventories in North America: A Critical Assessment. *J. Air Waste Manage. Assoc.* 56: 1115–29.

NARSTO (2005). *Improving Emission Inventories for Effective Air Quality Management across North America*, Pasco, Washington.

Petzold, A., Rasp, K., Weinzierl, B., Esselborn, M., Hamburger, T., Dörnbrack, A., Kandler, K., Schütz, L., Knippertz, P., Fiebig, M. and Virkkula, A. (2009). Saharan Dust Absorption and Refractive Index from Aircraft-based Observations during SAMUM 2006. *Tellus Ser. B* 61: 118–130.

Pope, C. and Dockery, D. (2006). Health Effects of Fine Particulate Air Pollution: Lines That Connect. *J. Air Waste Manage. Assoc.* 56: 709 –742.

Seinfeld, J.H., Carmichael, G.R., Arimoto, R., Conant, W.C., Brechtel, F.J., Bates, T.S., Cahill, T.A., Clarke, A.D., Doherty, S.J., Flatau, P.J., Huebert, B.J., Kim, J., Markowicz, K.M., Quinn, P.K., Russell, L.M., Russell, P.B., Shimizu, A., Shinozuka, Y., Song, C.H., Tang, Y.H., Uno, I., Vogelmann, A.M., Weber, R.J., Woo, J.H. and Zhang, X.Y. (2004). ACE-ASIA: Regional Climatic and Atmospheric Chemical Effects of Asian Dust and Pollution. *Bull. Am. Meteorol. Soc.* 85: 367–380.

Sokolik, I., Andronova, A. and Johnson, T.C. (1993). Complex Refractive Index of Atmospheric Dust Aerosols. *Atmos. Environ.* 27: 2495–2502.

Storelvmo, T., Hoose, C. and Eriksson, P. (2011). Global Modeling of Mixed-phase Clouds: The Albedo and Lifetime Effects of Aerosols. *J. Geophys. Res.* 116: D05207.

U.S. EPA (2000). Meteorological Monitoring Guidance for Regulatory Modeling Applications.

U.S. EPA (2015a). Emissions Factors & AP 42, Compilation of Air Pollutant Emission Factors. http://www.epa.gov/ttnchie1/ap42. (Accessed February 2015).

U.S. EPA (2015b). Emissions Inventories. http://www.epa.gov/ttn/chief/eiinformation.html. (Accessed February 2015).

Varma, R.M., Hashmonay, R.A., Du, K., Rood, M.J., Kim, B.J. and Kemme, M.R. (2006). A Novel Method to Quantify Fugitive Dust Emissions Using Optical Remote Sensing. In *Advanced Environmental Monitoring*, Platt, U. and Kim, Y. (Eds), Springer-Verlag GmbH, p. 143–154.

Watson, J.G. and Chow, J.C. (2000). Reconciling Urban Fugitive Dust Emissions Inventory and Ambient Source Contribution Estimates: Summary of Current Knowledge and Needed Research. DRI Document No. 6110.4F.

Watson, J.G. (2002). Visibility: Science And Regulation. *J. Air Waste Manage. Assoc.* 52: 628–712.

Yuen, W., Johnsen, D.L., Koloutsou-vakakis, S., Rood, M.J., Byung, J. and Kemme, M.R. (2014). Open Burning and Open Detonation PM_{10} Mass Emission Factor Measurements with Optical Remote Sensing. *J. Air Waste Manage. Assoc.* 64: 227–234.

Received for review, December 5, 2014
Revised, February 25, 2015
Accepted, February 28, 2015